10.1109/ULTSYM.2015.0314

# Visualization of the intensity field of a high intensity focused ultrasound (HIFU) source *in situ*

Trong Nguyen, Minh Do, *Fellow*, IEEE, Michael L. Oelze, *Senior Member*, IEEE
Department of Electrical and Computer Engineering
University of Illinois at Urbana-Champaign
Urbana, IL

*Abstract*— **High intensity focused ultrasound (HIFU) can provide a means of noninvasive ablation of tissues such as tumors. However, currently the gold standard for monitoring HIFU is MRI temperature mapping. Because of the expense, lack of portability and slow update of temperature maps from MRI, ultrasonic solutions to monitoring of HIFU remain an important clinical goal. Real-time visualization of the field distribution of the HIFU source during treatment would allow the localization of the intersection of the beam with the tissue. Real-time visualization of the beam in the context of the tissue is important for proper placement of therapy especially during tissue motion. To visualize the HIFU field in a tissue, a reconstruction technique was employed using a Fourier-domain f-k migration approach with a linear array system co-aligned with the HIFU source. The reconstruction technique used the scattered signal from the medium to reconstruct the intensity field pattern of the HIFU field *in situ* and superimpose the intensity field image on a B-mode of the scattering medium. A 6-MHz single-element transducer (f/3) was used as the HIFU source and aligned perpendicular to the field of a linear array (L14-5) operated by a SonixRP system equipped with a Sonix-DAQ. The array had 128 elements and a measured center frequency of 6.5 MHz. The 6-MHz HIFU source was pulse excited and the fields scattered from a sample, i.e., a homogeneous tissue-mimicking phantom or a chicken breast, were received by each element of the linear array. Beam forming based on Fourier-domain f-k migration techniques were applied to the channel data to reconstruct the intensity field pattern from the HIFU source. For comparison, a wire target was placed in the field and the intensity field pattern was reconstructed by moving the wire throughout the focal region. The intensity field pattern reconstructed from the sample was compared to the field characteristics of the 6-MHz source characterized by the wire technique. The intensity field pattern was then superimposed on a registered B-mode image of the sample acquired using conventional B-mode imaging with the linear array and the SonixRP to provide context to the therapy beam placement. The beam width estimates at the HIFU focus using the *in situ* reconstruction technique and the wire technique were 1.7 mm and 1.5 mm, respectively. The depth of field estimates for the *in situ* reconstruction technique and the wire technique were 20.1 mm and 19.0 mm, respectively. Therefore, the novel reconstruction technique was able to accurately visualize the field of a focused source in the context of the interrogated medium. The visualization technique would allow real-time adjustment of the HIFU beam location in tissues during therapy.**

***Keywords—Beam forming; High intensity focused ultrasound; Field visualization, Stolt f-k migration***

## I. Introduction

Focused ultrasound continues to be explored for non-invasive treatment of various diseases including cancer, Parkinson's disease and Alzheimer's [1-3]. The idea behind using focused ultrasound to treat disease is that ultrasonic waves can be focused to a particular location, the energy of the ultrasound absorbed in the focal region and the resulting heat used to preferentially kill tissues in the focal region. The strength of the using focused ultrasound is the ability to target specific tissue regions with the focusing of ultrasonic waves, noninvasively. Specific tissues can be targeted for treatment while surrounding healthy tissues can be spared the therapy.

However, several drawbacks still exist for more extensive use of focused ultrasound for therapy. The major drawback in using focused ultrasound for non-invasive therapy is the difficulty in monitoring the placement of the focused ultrasound beam and the temperature elevations produced by the exposure. Currently, MRI is used to guide focused ultrasound applications (MRgFUS) [4]. MRI is capable of producing maps of temperature elevations at near real time. However, MRI is still sensitive to tissue motion and the costs of using MRI with a compatible focused ultrasound system are very high. Therefore, the development of less expensive, robust methods for monitoring the application of focused ultrasound is still warranted and medically significant.

In this study, a technique for rapidly visualizing the beam from a focused ultrasound source *in situ* is developed and demonstrated in tissue mimicking phantoms. The underlying principle is that an array imaging probe co-aligned with a focused ultrasound source can be used to reconstruct the focused ultrasound field *in situ*. To optimize the visualization of the field from the focused ultrasound source for application in therapy, it is important to rapidly reconstruct the field with the highest spatial resolution possible that can be produced by the array-imaging probe.

## II. Methods

### A. Experimental configuration

To visualize the beam from a focused ultrasound source, a linear imaging array probe, i.e., a L14-5, was aligned with a single-element focused ultrasound transducer (f/3). The L14-5 linear array probe was operated by a SonixRP system (Ultrasonix Medical Corp., Richmond, BC, Canada) with a SonixDAQ. The SonixDAQ allowed for the radio frequency (RF) data to be acquired from each element of the array pre-

This work was supported in part by grants from the National institutes of Health (NIH): R01EB008992.

beamforming. The array had a center frequency of 6 MHz as estimated from a wire target. The array had 128 elements, a total length of 38 mm and element size of 0.2798 x 4 mm. The imaging plane of the linear array was aligned with the focus of the focused ultrasound transducer and the array and focused ultrasound source were at 90° from each other. The single-element focused ultrasound source had a center frequency of 6 MHz.

A tissue-mimicking phantom providing uniform speckle was placed at the focus of the focused ultrasound transducer. The tissue-mimicking phantom was made from agar with glass beads uniformly embedded throughout the phantom volume to produce scattering of the ultrasound. The focused ultrasound transducer was pulse excited using a Panametrics 5800 pulser/receiver (Olympus NDT, Waltham, MA). Figure 1 illustrates the experimental configuration. Once the focused ultrasound transducer was pulse excited, the fields from the focused ultrasound transducer were scattered by glass beads in the tissue-mimicking phantom. The imaging array was triggered in sync with the pulsed excitation and received echoes were acquired from each element of the array. The array acted as a passive listening device. The fields scattered from many sub-resolution scatterers in the phantom were recorded by the array. The acquired data were then processed to visualize the beam *in situ*. After demonstrating the technique in a tissue-mimicking phantom, the techniques were also applied to a chicken breast sample.

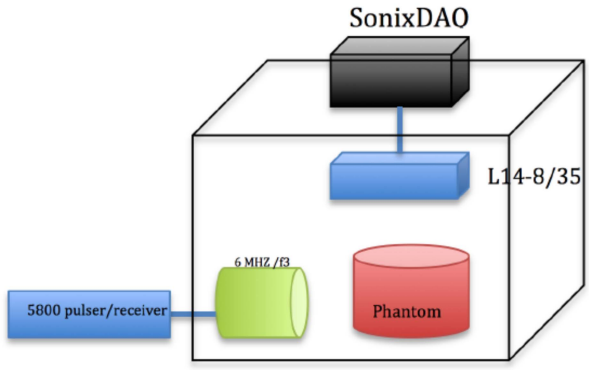


**Figure 1. Experimental configuration.**

*B. Beam Reconstruction Methods*

Two approaches were used to reconstruct the scattered field from the phantom. The first approach utilized a traditional delay and sum to focus the received signal at each location in the imaging plane. For each pixel $(x_f, z_f)$ in the beamformed image, the delay time from a channel was calculated as,

$$t_i = \frac{\sqrt{(x_f - x_i)^2 + (z_f - z_i)^2}}{c} \qquad (1)$$

where $c$ is the sound speed assumed to be 1540 m/s and $i$ is the array element index for the array point coordinate for an array element $(x_i, z_i)$. The beamformed pixel value was calculated as

$$I(x_f, z_f) = \sum_{i=1}^{128} s_i\left[\frac{z_f}{c} - t(i)\right] \qquad (2)$$

where $s_i[n]$ is the channel data from element $i$. The delayed sample was usually not an integer, thus linear interpolation was used between the two closest integer samples to compute the added value. A pixel represented a small area of 1 X 1 mm. Each pixel was stitched together to provide the full image.

In the second approach, focusing of the full field on receive was achieved using Stolt's f-k migration for a bistatic setup. This was adapted from the Garcia's development for plane wave insonification [5]. The exploding reflector model (ERM) assumes all the acoustic sources exploding simultaneously. The f-k migrations allow reconstruction of those sources given the wave field on the surface of the transducer. To account for the two-way propagation in plane wave imaging, transformation of the exploding sources location and speed of sound is made to produce the same delay hyperbola profile. For example, in the case of one emitter-receiver, a scatterer $(x_s, z_s)$ produces a two-way travel time hyperbola in the form of

$$\tau_s(x) = \frac{2}{c}\sqrt{(x_s - x)^2 + {z_s}^2} \qquad (3)$$

while the exploding source at $(\hat{x}_s, \hat{z}_s)$ in a medium with sound speed $\hat{c}$ produces a delay time of:

$$\tau_s(x) = \frac{1}{\hat{c}}\sqrt{(\hat{x}_s - x)^2 + {\hat{z}_s}^2}. \qquad (4)$$

Choosing the ERM sound speed to be half the real sound speed and keeping the same scatterer locations makes the two delay hyperbolas the same for both transmit and receive. For the general case of a tilted plane wave, simple transformation of the sound speed and scatterer locations exists if the insonification angle is small. In the bistatic setup, we assumed the ERM after compensation for the travel time from the single-element focused transducer to the scatterer near the focus, thus Stolt's fk migration can be used to reconstruct the passive map. This has the advantage of fast reconstruction in the Fourier domain and full field focusing without stitching images together compared to the delay and sum approach.

*C. Field Characterization of the Focused Ultrasound Source*

To quantify the performance of the technique to reconstruct the beam from the focused ultrasound source, a wire technique was first used to characterize the field properties of the focused ultrasound source. A tungsten wire with diameter of 38 μm was placed at the focus of the focused ultrasound source, i.e., the 6 MHz f/3 single-element transducer. Because the predicted beamwidth of the single-element source used as the focused ultrasound transducer was only 0.75 mm, a special holder was made to align the single-element focused transducer beam and the imaging plane of the receiving array. The holder, which holds the single-element focused transducer and the receiving array was connected to a

micro-precision positioning system (Daedal Inc. Harrison City, PA). The wire was moved through the focal region of the single-element focused transducer with an axial dimension of 20 mm and lateral dimension of 1 mm. The scanning grid was centered at the focus of the single-element focused transducer. The axial scanning step was 0.5 mm and the lateral scanning step was 0.1 mm. For each step, the single element was excited using a Panametrics 5800 pulser-receiver. The scattered signal was received by the linear array (L14-5) operated by the SonixRP system equipped with a SonixDAQ. The excitation of the single-element focused transducer and the receiving outset of the linear array were synchronized. The pre-beamformed data acquired by the SonixDAQ was downloaded to a hard-drive and post processed.

## III. Results

Figure 2 shows the map of the beam generated by moving the wire through the focus region of the single-element focused transducer. The single-element focused transducer was pulse excited and the array passively listened to the returns coming from the wire target as it moved through the field of the focused transducer. The delay and sum approach was used to focus the passive array at each location of the wire to create the field map. Figure 2(b) is the delay-corrected image of the Fig. 2(a). Because the delay correction is an approximate process, we use Fig. 2(a) to estimate the -6-dB beamwidth of the single element. A red ellipse was drawn on Fig. 2(a) to visualize the -6-dB beamwidth. The -6-dB beamwidth was estimated to be 1.5 mm and the -6-dB depth of field was estimated to be 19 mm. Table I lists the estimated beam parameters from the wire target and the phantom reconstructions.

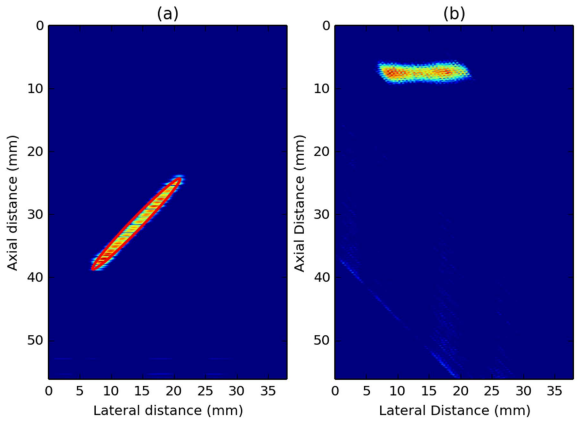


**Figure 2. Passive map of the focused field of the wire (a) before and (b) after correction.**

Figure 3 shows the reconstructed image of the beam from the single-element focused transducer reconstructed from the scattered fields produced in the tissue-mimicking phantom. Figure 3 (a) is the beamformed image after using just one transmit-receive event. As before, the single-element focused transducer is pulse excited once and the fields scattered from throughout the phantom are received by the listening array. Focusing on receive is used to reconstruct each point in the field and visualize the beam of the focused source.

**TABLE I: Comparison between the wire target and agar phantom -6-dB beamwidth and depth of field.**

| | Wire target | Agar phantom |
|---|---|---|
| **Beamwidth** | 1.5 mm | 1.7 mm |
| **Depth-of-field** | 19 mm | 20.1 mm |

Figure 3 (b) shows a compounded image using five consecutive snapshots from different independent planes in the phantom. The speckle of the reconstruction is smoothed by compounding the beam reconstruction from independent samples. However, this requires more than one transmit receive event. Figure 3 (c) is the corrected image of Fig. 3 (b). As in the case of the wire, the beamwidth was estimated using the pre-corrected beamformed image. The -6-dB beamwidth estimate was 1.7 mm and the -6-dB depth of field was estimated to be 20.1 mm (see Table I).

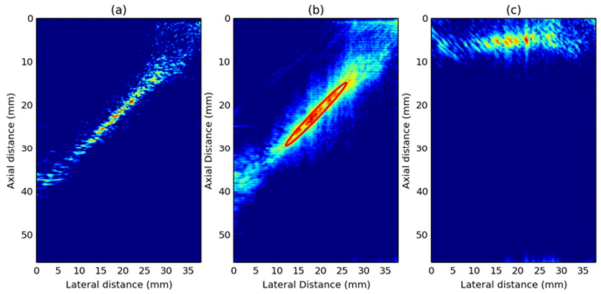


**Figure 3. (a) Beamformed image of one transmit-receive event. (b) Beamformed image of the beam in the phantom by compounding five transmit-receive events. (c) Delay-corrected image of Fig. 3 (b).**

Figure 4 shows the position of the delay-corrected compounded beam of the single-element focused transducer overlaid on the B-mode image. The beam can be visualized *in situ* within the phantom and is denoted by the color whereas the phantom is in grayscale.

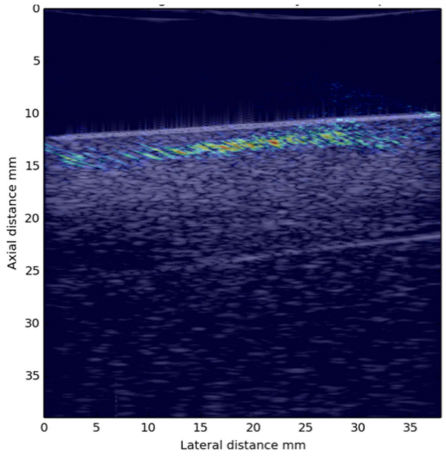


**Figure 4. Overlaid beam on the B-mode of the agar phantom.**

Figure 5 shows the reconstructed beam in the phantom when using the Stolt's fk migration and delay and sum. Compared to the delay and sum procedure, the computational time was greatly reduced. Furthermore, because the reconstructed image using the Stolt fk migration was not stitched together, as was done for the delay and sum image, the reconstruction has a smoother appearance.

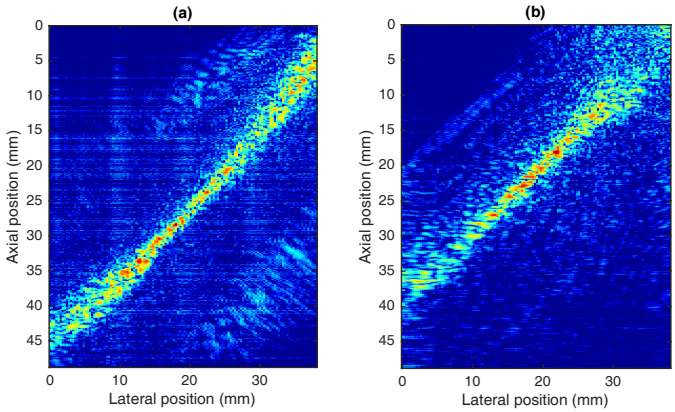


**Figure 5. (a) Stolt's fk beamforming of the beam in agar phantom and (b) the delay and sum reconstruction using the same data.**

Figure 6 shows the reconstructed beam of the single-element focused transducer when insonifying a chicken breast. The same scatterers in the chicken breast that produce speckle were used to provide the beam reconstruction. The beam was visualized within the chicken breast and could be used to monitor beam placement for focused ultrasound therapy.

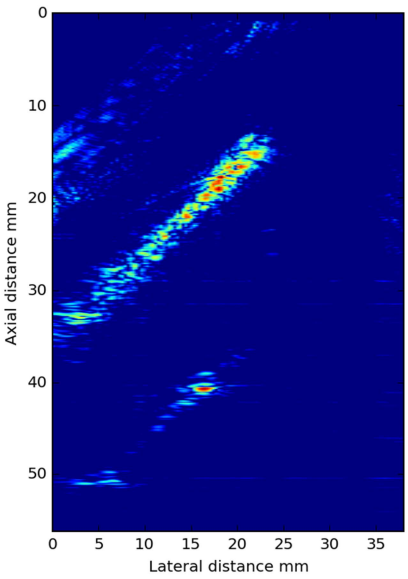


**Figure 6. Reconstructed passive beam in the chicken breast.**

## IV. Discussion

A novel mapping technique was demonstrated that allowed the reconstruction of the beam field from a focused source *in situ*. The reconstruction had beam properties that corresponded well to properties defined by characterization using a wire target. The nominal -6-dB beamwidth of the single-element transducer was 1.4 mm and the -6-dB beamwidth estimate from the wire target mapping was 1.5 mm.

The passive mapping of scatterers in the agar phantom was equivalent to the wire mapping except the whole field throughout the beam could be acquired using a single excitation. Compounding appeared to smooth out the representation of the field. The -6-dB beamwidth representation was not continuous but rather appeared as a speckle pattern. Therefore, the more images used in the compounding, the clearer the pattern of the beam emerged.

The reconstructed field could be superimposed on B-mode images to give anatomical context of the location of the focused transducer beam in a tissue. Furthermore, bright spots in the corresponding B-mode image could be used to correct for image intensity variations in the field pattern due to structures in the tissues like bright specular scatterers or tissue interfaces.

We did not measure the beam characteristics in the chicken breast setup due to the weak signal. Future experiments to enhance the signal will produce better estimates of the beam. The pre-beamformed data were processed offline due to the capabilities of the SonixDAQ. The time domain beamforming could not be real time due to the computational load. However, the Stolt f-k migration code can achieve real-time beamforming.

## V. Conclusion

A liner array imaging probe was aligned with a focused ultrasound transducer in order to visualize the focused ultrasound beam *in situ*. To reconstruct the field from the focused ultrasound transducer a Stolt f-k migration technique was used to focus the field on receive. The resulting visualizations from the Stolt f-k migration were improved over conventional delay and sum. The visualized beam properties were similar to properties characterized using a wire technique.

## References


[1] J. E. Kennedy, "High-intensity focused ultrasound in the treatment of solid tumours," *Nature reviews. Cancer,* vol. 5, pp. 321-7, Apr 2005.

[2] Focused ultrasound treatment of various conditions http://www.fusfoundation.org/diseases-and-conditions/overview, Accessed (10/6/2015).

[3] Y. F. Zhou, "High intensity focused ultrasound in clinical tumor ablation," *World journal of clinical oncology,* vol. 2, pp. 8-27, Jan 10 2011.

[4] B. Quesson, C. Laurent, G. Maclair, B. Denis de Senneville, C. Mougenot, M. Ries, T. Carteret, A. Rullier, and C. T. W. Moonen, "Real-time volumetric MRI thermometry of focused ultrasound ablation in vivo: a feasibility study in pig liver and kidney," *NMR in biomedicine,* vol. 24, pp. 145-153, 2011.

[5] D. Garcia, L. L. Tarnec, S. Muth, E. Montagnon, J. Por´ee, and G. Cloutier, "Stolts f-k Migration for Plane Wave Ultrasound Imaging," IEEE Trans. Ultrason., Ferroelect., Freq. Control, vol. 60, no. 9, pp. 1853–1867, 2013.